

Bendability parameter for twisted ribbons to describe longitudinal wrinkling and delineate the near-threshold regime

Madelyn Leembruggen,^{1,*} Jovana Andrejevic,^{2,†} Arshad Kudrolli,^{3,‡} and Chris H. Rycroft^{4,5,§}

¹*Department of Physics, Harvard University, Cambridge, MA 02138, USA*

²*Department of Physics, University of Pennsylvania, Philadelphia, Pennsylvania 19104, USA*

³*Department of Physics, Clark University, Worcester, Massachusetts 01610, USA*

⁴*Department of Mathematics, University of Wisconsin–Madison, Madison, WI 53706, USA*

⁵*Computational Research Division, Lawrence Berkeley Laboratory, Berkeley, CA 94720, USA*

We propose a dimensionless bendability parameter, $\epsilon^{-1} = [(h/W)^2 T^{-1}]^{-1}$ for wrinkling of thin, twisted ribbons with thickness h , width W , and tensional strain T . Bendability permits efficient collapse of data for wrinkle onset, wavelength, critical stress, and residual stress, demonstrating longitudinal wrinkling’s primary dependence on this parameter. This new parameter also allows us to distinguish the highly bendable range ($\epsilon^{-1} > 20$) from moderately bendable samples ($\epsilon^{-1} \in (0, 20]$). We identify scaling relations to describe longitudinal wrinkles that are valid across our entire set of simulated ribbons. When restricted to the highly bendable regime, simulations confirm theoretical near-threshold (NT) predictions for wrinkle onset and wavelength.

Wrinkling of geometrically frustrated sheets is a well-studied subject. Recently, systematic treatments of thin sheet wrinkling examined flat sheets on compressed substrates [1, 2] and frustrated annuli [3–6], which possess tractable axial symmetries. Next thin films were floated on deformable fluid surfaces [7–13] or adhered to curved planes [14–16], further complicating the forces and geometries complicit in wrinkle formation. Even deflated balloons [17] have had their wrinkles poked and measured. Many features of such wrinkled sheets have been successfully described using near-threshold (NT) approximations which take the amplitude of the wrinkling as a small perturbation from the flat reference state [4, 5, 13]. In some cases it was helpful to approach the problem using a far-from-threshold (FT) expansion which assumes the compressive stress in the sheet is alleviated to first order by the appearance of wrinkles [1, 4–6, 12, 14–16].

A thin ribbon when twisted also develops wrinkles due to geometric frustration. Wrinkled ribbons were first documented in the 1930s [18], but the existence of the longitudinally wrinkled phase was not verified numerically until nearly 50 years later [19]. Since then, twisted ribbons have been theoretically analyzed [20–22], and their phase space has been experimentally mapped [23]. We have previously shown that simulations can replicate the morphology and mechanics of ribbons buckled and wrinkled via twisting [24] and investigated NT and FT predictions across a broad swath of the parameter space. Despite some of the successes of both NT and FT approximations for the twisted ribbon [20, 21, 25], the transition between their regimes of validity remains elusive and exact predictions for onset of wrinkling, their extent and wavelength lacking [24]. Simulations offer a grip on ribbons that are neither very thin nor free of compressive stress, with potential to illuminate the murky demarcation of NT and FT predictions.

Bendability Parameter— A thin, twisted ribbon develops longitudinal wrinkles along its center when a longi-

tudinal force F and end-to-end twist θ are applied, as shown via simulated ribbons in Fig. 1(a). The wrinkles have wavelength λ_{lon} and are confined to a portion of the ribbon called the “wrinkled zone”, which is symmetric about the center line with width $2r_{\text{wr}}$, labeled in Fig. 1(b).

The two dimensionless parameter groupings useful for analyzing wrinkling in other thin sheets, such as frustrated annuli or floating films, are the confinement (here called α) and the bendability (ϵ^{-1}) [4, 5, 12–16, 26]. In the case of twisted ribbons, the appropriate confinement parameter was previously identified [21]:

$$\alpha \equiv \frac{\eta^2}{T} \quad (1)$$

where η represents the geometric strain, and T the tensional strain. η and T are themselves dimensionless, with

$$\eta = \theta \frac{W}{L}, \quad T = \frac{F}{EhW}, \quad (2)$$

where E is the Young’s modulus, h is the ribbon thickness, W the ribbon width, and L the ribbon length.

On the other hand, bendability for the twisted ribbon, the dimensionless ϵ^{-1} , has not yet been identified in the literature. We propose

$$\epsilon \equiv \frac{12(1-\nu^2)B}{WF} = \left(\frac{h}{W}\right)^2 \frac{1}{T} \quad (3)$$

as the definition of inverse bendability for twisted ribbons, where ν is Poisson’s ratio and B is the bending modulus.

Previous studies that use bendability, such as [4, 5, 12–16, 26], focus primarily on the limit of highly bendable sheets, such that $\epsilon^{-1} \gg 1$. Many of our ribbon samples, however, fall into a “moderately” bendable range with $\epsilon^{-1} \in (0, 20]$. We first identify scaling laws that apply to the full range of our samples, then examine only the highly bendable sheets ($\epsilon^{-1} > 20$) to compare directly to theoretical NT estimates.

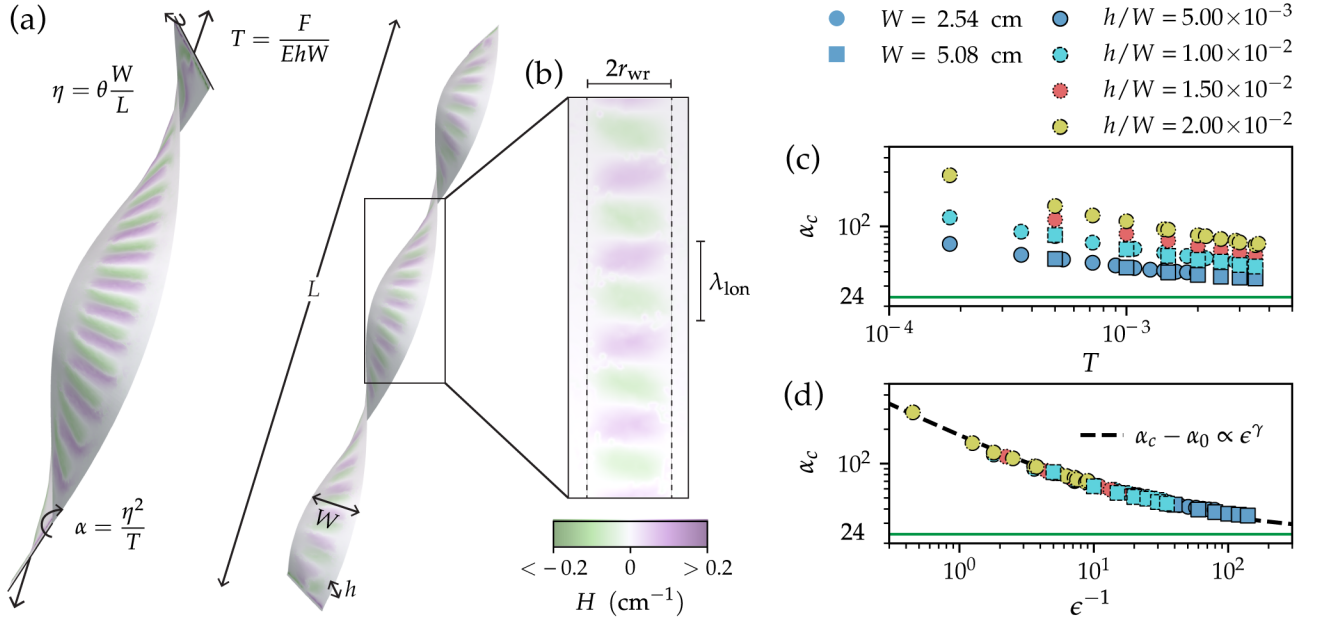


FIG. 1. (a) Observed snapshots of wrinkled ribbons with width $W = 5.08$ cm (left) and 2.54 cm (right) held at various tensions T and twisted by an amount η are displayed here, both with thickness $h = 0.254$ mm and held at $T = 2.5 \times 10^{-3}$. Overlaid in purple (green) is the mean curvature H of the ribbon, buckled above (below) the plane. (b) The ribbon projected on a flat plane with H rendered according to color map shows the wrinkling is confined to a region of width $2r_{wr}$, marked here by vertical dashed lines, and has a wavelength λ_{lon} . (c) The critical confinement, α_c , at which the wrinkles appear plotted against the longitudinally applied tension. An infinitely thin ribbon would develop wrinkles at confinement $\alpha_0 = 24$ (solid green line). Ribbons with finite thickness, however, transition to the wrinkle state at $\alpha_c > \alpha_0$. (d) α_c versus the bendability parameter, defined in Eq. (3), with data collapsing onto the line $\alpha_c - \alpha_0 \propto \epsilon^\gamma$ with $\gamma = 0.585 \pm 0.004$.

Simulation Details— Our ribbons are simulated by sheets comprised of an underlying topology of either 11250 or 22500 randomly distributed nodes connected by in-plane springs, and bending between adjacent facets is quadratically penalized similar to the Seung-Nelson model [27]. Both the in-plane stretching and out-of-plane bending models have been generalized for the random mesh using modifications adapted from Van Gelder/Lloyd [28, 29] and Grinspun [30, 31], respectively. Full derivation and validation of the mesh model are presented by Leembruggen, *et al.* [24].

As a force-based model, interactions between nodes are described purely by Newton’s second law. We integrate the resultant system with an implicit-explicit integration scheme that automatically switches between methods based on the magnitude of the acceleration of nodes in the sheet [32]. Since the ribbon is usually in the quasi-static limit where $F \approx 0$, we primarily use an implicit integration scheme. However, an explicit integrator is triggered during frames with large acceleration, such as transverse buckling events. A typical ribbon simulation requires a wall-clock time of 8 h, using 8 threads on a Linux computer with dual 2.40 GHz Intel Xeon E5-2630 CPUs.

Six ribbons with $L = 45.7$ cm were used in this study: two of width $W = 5.08$ cm with thicknesses $h/W =$

$5 \times 10^{-3}, 10^{-2}$; and four of width $W = 2.54$ cm with thicknesses $h/W = 5 \times 10^{-3}, 1 \times 10^{-2}, 1.5 \times 10^{-2}, 2 \times 10^{-2}$. The Young’s modulus for these ribbons was $E = 3.4$ GPa, and Poisson’s ratio was $\nu = 1/3$, fixed by the triangular structure of the underlying mesh [27, 29]. These ribbons were held at various fixed tensions, T , within the longitudinal buckling phase. Ultimately we had 96 samples of longitudinally wrinkled ribbons with varying λ_{lon} .

Wrinkling Onset— Examining the ribbon’s stress in the longitudinal (y) direction [21],

$$\frac{\sigma^{yy}(x)}{T} = 1 + \frac{\alpha}{2} \left(\left(\frac{x}{W} \right) - \frac{1}{12} \right), \quad (4)$$

identifies $\alpha_0 = 24$ as the confinement at which the stress becomes compressive along $x = 0$ (the ribbon’s spine). An infinitely thin ribbon, unable to support compressive stress, buckles at α_0 . But ribbons with thickness support small amounts of stress, and thus buckle at confinements $\alpha_c > \alpha_0$, as demonstrated across samples in Fig. 1(d). Previous estimates of this finite thickness correction based on experiments followed the form $\eta_c = \eta_0 + C_{lon} \frac{h}{W}$ where $\eta_0 = \sqrt{24T}$ coincides with $\alpha_0 = 24$ [23]. Written in terms of the confinement parameter we propose, this translates to a correction on the order of $\alpha_c - \alpha_0 \propto \epsilon$. However, as plotted in Fig. 1(e), we observe

$$\alpha_c - \alpha_0 \propto \epsilon^\gamma, \quad (5)$$

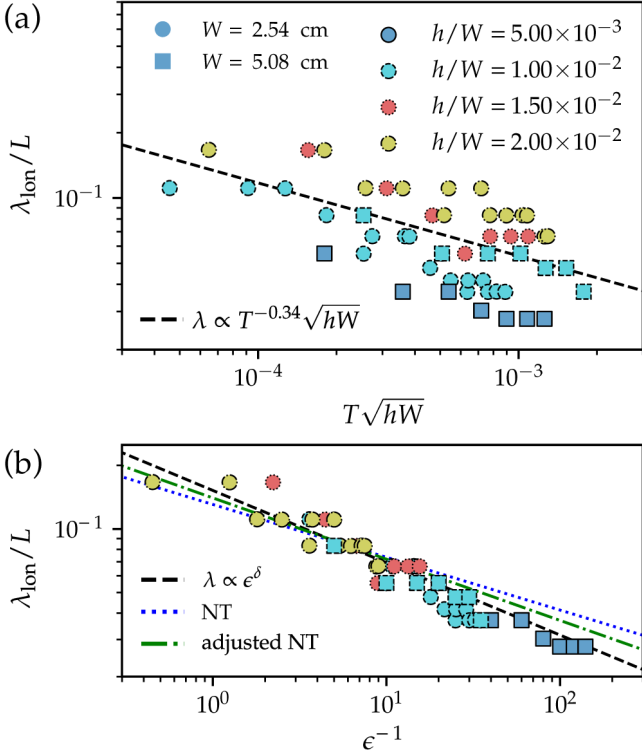


FIG. 2. (a) The wavelength per unit length as a function of the ribbon's dimensions and applied tension and comparison with NT analyses (dashed black line) [20, 21]. Plotted with this normalization, the data are broadly distributed. (b) Plotted against bendability, the wavelengths collapse more closely. In terms of ϵ^{-1} , the theoretical NT analyses [20, 21] predict $\delta = 1/4$, plotted by the blue, dotted line. Adjusting the NT approximation by substituting the value for γ observed in Fig. 1(e), such that $\delta = \gamma/2 = 0.293 \pm 0.002$ is shown here by the green, dash-dotted line. Note that points with $\epsilon^{-1} > 20$ roughly follow the slope of the NT prediction, but diverge from this line when $\epsilon^{-1} < 20$.

with $\gamma = 0.585 \pm 0.004$. Moreover, we find that it additionally depends on tension. As shown by the data collapse in Fig. 1(e) the tension dependence along with the geometric parameters are captured by the bendability parameter introduced in Eq. (3). The previously proposed correction overcompensated for the thickness of the ribbon; rather a correction of $\mathcal{O}(\epsilon^{1/2})$ should be applied directly to the α parameter, not to η . Chopin *et al.* posit that, using the NT approximation, $(\alpha_c - \alpha_0) \sim (h/W)T^{-1/2}$ [21]. Recast using ϵ^{-1} , the equivalent prediction is $\alpha_c - \alpha_0 \propto \epsilon^\gamma$ with $\gamma = 1/2$.

Since the wavelength at onset of longitudinal wrinkling is the same at larger α , we wait until the wrinkle pattern has developed appreciable amplitude before measuring λ_{lon} to make the measurement more precise [24]. NT approximations have been used to estimate wavelength at onset [20, 21]: $\lambda \propto r_{\text{wr}} \propto \sqrt{h/W}T^{-1/4}$, and were noted to describe experimentally measured wavelengths [23].

In Fig. 2(a) we plot the wavelength per unit length (i.e. the inverse of preferred wave number) using the same normalization as Chopin and Kudrolli's experiment [23]. Also plotted in this figure is a best fit as a function of T , represented by the black, dashed line. The vertical spread in these data suggests that the dependence on h and W is not captured by the \sqrt{hW} normalization. However, plotting wavelengths against the bendability, in Fig. 2(b), the values collapse, scaling as $\lambda_{\text{lon}}/L \propto \epsilon^\delta$ with $\delta = 0.342 \pm 0.019$, shown as a black, dashed line.

Recast in terms of bendability, the theoretical NT prediction for wavelength is $\lambda_{\text{lon}}/L \propto (\alpha_c - \alpha_0)^{1/2} \propto \epsilon^\delta$, with $\delta = \gamma/2 = 1/4$ in this case. Alternatively we could assume adjusting γ propagates forward to other NT predictions. In which case, $\delta = \gamma/2 = 0.293 \pm 0.002$, using Eq. (5). In Fig. 2(b), we plot the theoretical NT $\delta = 1/4$ in a blue, dotted line, and adjusted NT $\delta = 0.293$ in a green, dash-dotted line.

All in all, we find that the scaling λ_{lon} in terms of ϵ^{-1} is a vast improvement over past investigations of wavelength versus tension. Regardless of the precise slope of this collapse, the points themselves are clustered more closely than in previous studies [24], further affirming the usefulness of ϵ .

Residual Stress— Throughout the simulation we extract the stress tensor via the deformation gradient tensor for the underlying mesh [24]. Longitudinal slices are taken along the middle third of the ribbon, then averaged along the longitudinal direction (y) to obtain the quantity $\langle \sigma^{yy}(x) \rangle_y$. Instinctually, one might expect the critical buckling stress $\langle \sigma_c^{yy}(0) \rangle_y$ is proportional to the cross-sectional area ($hW/W^2 = h/W$ in dimensionless units). In Fig. 3(a) we plot critical stress at $x = 0$ against this candidate scaling factor. This simple estimate, however, results in incomplete collapse of the data.

Turning back to our stress equation, Eq. (4), along $x = 0$ we expect the stress at $\alpha > \alpha_0$ to be

$$\frac{\sigma^{yy}}{T} = 1 - \frac{\alpha}{24} = 1 - \frac{\alpha_0}{24} - \frac{\alpha - \alpha_0}{24} = -\frac{\alpha - \alpha_0}{24}. \quad (6)$$

Since we observe the scaling for confinement in Eq. (5), critical stress should go as

$$\frac{\sigma_c^{yy}}{T} = -\frac{\alpha_c - \alpha_0}{24} \propto -\epsilon^\gamma. \quad (7)$$

This is consistent with our measurements, plotted in Fig. 3(b), which find $\sigma_c^{yy}/T \propto -\epsilon^{\gamma'}$, with the measured $\gamma' = 0.599 \pm 0.006$.

It is not clear from analytical studies whether the ribbon's residual, post-buckling, compressive stress should scale the same way as its critical stress, especially as $\alpha > \alpha_c$ changes [16, 33]. However, as shown in Fig. 3(c), stress saturates at values very close to the critical stress; we measure $\gamma'_{\text{res}} = 0.591 \pm 0.003$.

The Boundary of Near Threshold— It is expected that the NT relations are valid only for highly bendable sheets

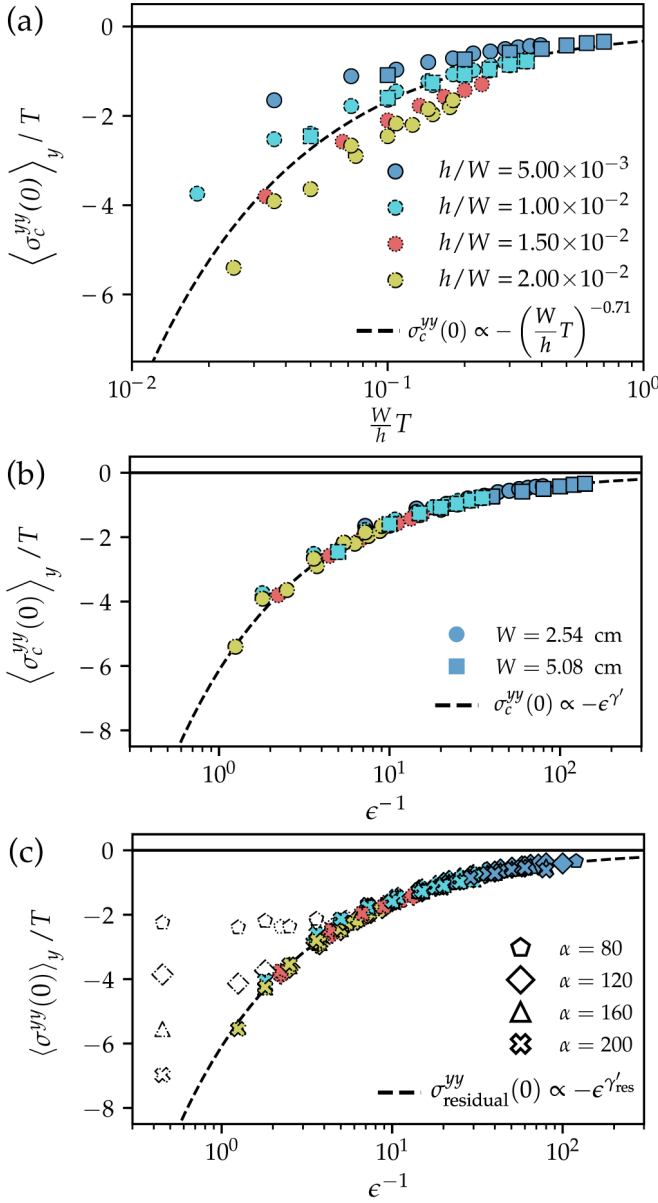


FIG. 3. (a) The critical stress along the ribbon center at the onset of wrinkling plotted against $\frac{W}{h} T$ results in incomplete collapse of the data. (b) When written as a function of bendability, the stress at the critical confinement follows the curve $\sigma_c^{yy}(0) \propto -\epsilon^{\gamma'}$, $\gamma' = 0.599 \pm 0.006$. This relationship follows from Eqs. (4) & (7). (c) The stress of each ribbon sample at four different confinements, α , resulting in 384 points. Open markers indicate the stress in a ribbon before it has buckled, whereas filled markers indicate the stress post-buckling. Marker shape refers to the confinement, α , at which the stress was sampled. Post-buckling, the ribbons support residual stress. Residual stress saturates according to the bendability of the ribbon, and is independent of α . The post-buckling residual stress follows the relationship $\sigma_{\text{residual}}^{yy}(0) \propto -\epsilon^{\gamma'_{\text{res}}}$, $\gamma'_{\text{res}} = 0.591 \pm 0.003$, similar to the scaling of σ_c^{yy} in (b).

such that $(h/W)^2 \ll T$, or equivalently, $\epsilon^{-1} \gg 1$. Although there are no sharp transitions in the data of Figs. 1 & 2 as a function of ϵ^{-1} , we could exclude points with small bendability to better understand how confinement ($\alpha_c - \alpha_0$), wavelength (λ_{lon}), and critical stress ($\langle \sigma_c^{yy}(0) \rangle_y / T$) scale in the highly bendable limit.

In Fig. 4(a) we plot the value of the scaling exponents for confinement (γ) and wavelength (δ) as a function of the lower threshold, $\epsilon_{\text{lb}}^{-1}$. As $\epsilon_{\text{lb}}^{-1}$ increases, further restricting the data to a highly bendable range, we see γ changes little, hovering around the value 0.5. On the other hand, δ is quite sensitive to $\epsilon_{\text{lb}}^{-1}$, but converges to ≈ 0.25 when $\epsilon_{\text{lb}}^{-1} > 20$. Therefore, when constrained by a highly bendable limit, our simulations agree entirely with NT predictions that $(\alpha_c - \alpha_0)_{\text{NT}} \propto \epsilon^{1/2}$ and $\lambda_{\text{lon}}^{\text{NT}} \propto \epsilon^{1/4}$.

Figures 4(b-d) recreate Figs. 1(d), 2(b), & 3(b) respectively, this time restricting the data points such that only highly bendable ribbons are included in the fit of the scaling exponent. Excluded data are plotted with desaturated color, to the left of the vertical dotted lines, and included data are plotted at full saturation to the right of the cutoff line. With this threshold imposed, the confinement in Fig. 4(b) has $\gamma = 0.513 \pm 0.001$; wavelength in Fig. 4(c) has $\delta = 0.255 \pm 0.044$; and critical stress in Fig. 4(d) has $\gamma' = 0.608 \pm 0.029$. Interestingly, the critical stress remains largely unchanged when thresholded, and is inconsistent with the stress (Eq. (7)) expected using the thresholded confinement scaling.

Discussion—Inspired by studies of complementary wrinkled systems, we have introduced a dimensionless parameter for bendability of a twisted ribbon ϵ^{-1} . Specifically ϵ^{-1} incorporates the effect of finite thickness of the sheet, and extends predictions made concerning infinitely thin ribbons. Then, we demonstrate that ϵ^{-1} successfully describes the onset of wrinkling, wavelength of wrinkles, and even the stress along the center of the ribbon at and after the onset of wrinkles. By rewriting the NT and FT predictions [21] in terms of ϵ^{-1} , we show that the onset of wrinkling scales somewhere between the NT and FT predictions of [21], but more closely to the NT results. When the data are restricted to a highly bendable region ($\epsilon^{-1} > 20$), they exactly match NT predictions. Perhaps most successfully, ϵ^{-1} allows investigation of ribbons in the “moderately” bendable ($\epsilon^{-1} \in (0, 20]$) limit, which are less bendable than theoretically tractable ribbons. Including this broader set of bendabilities enables us to determine scaling laws which are valid for a wide range of wrinkled ribbons.

Further, analyzing simulated ribbons has also allowed us to extract the stress in the sheet throughout the twist, which is prohibitively difficult to measure in experiments. Thus, the simulations have revealed stress in finite-thickness ribbons is not completely alleviated by buckling as is assumed in FT analysis, and the compressive stress they support saturates at the critical buckling stress. Our simulations also demonstrate that critical

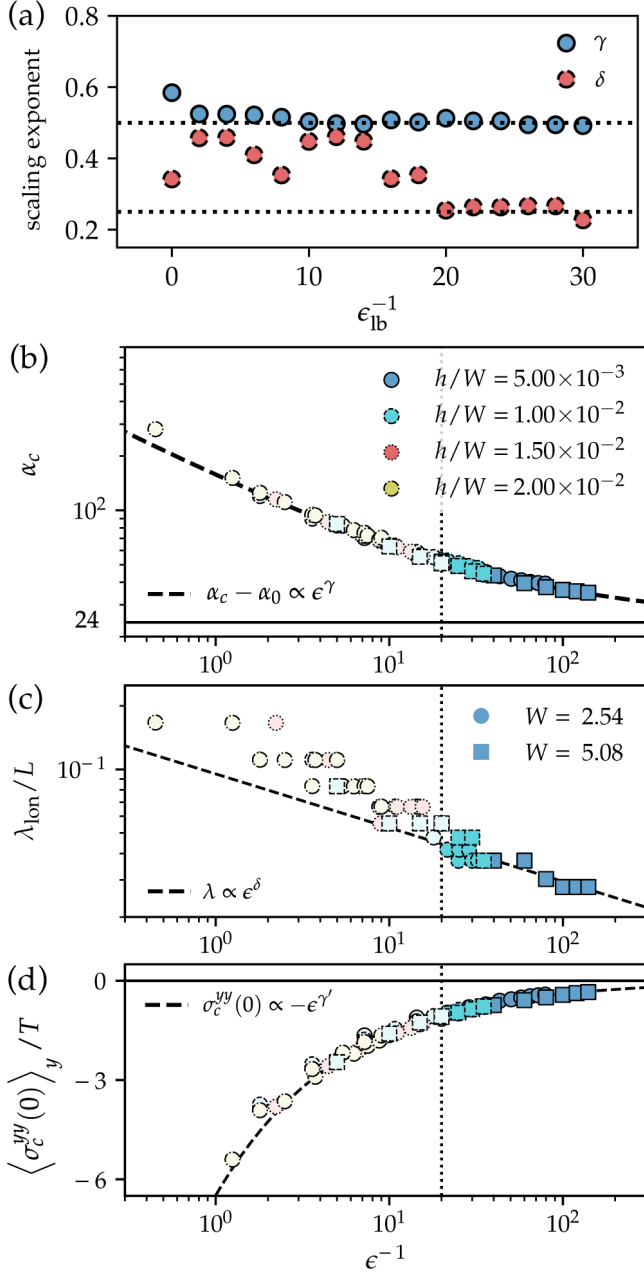


FIG. 4. (a) Various thresholds are placed on the lower bound of ϵ^{-1} . The scaling exponent, γ , of the confinement (upper, blue circles, solid border) remains largely unchanged as the lower bound changes. The wavelength exponent, δ (lower, red circles, dashed border), on the other hand, is more sensitive to the threshold of ϵ^{-1} ; when the threshold reaches $\epsilon_{lb}^{-1} \approx 20$, the $\delta \approx 0.25$. Horizontal lines are plotted at 0.25 and 0.5 to help guide the eye. (b–d) Replications of Figs. 1(d), 2(b) and 3(b) where the scaling exponent (dashed, black line) is fitted only using data with $\epsilon^{-1} > 20$. Darker points, to the right of the vertical dotted lines, are included in the scaling fit; desaturated points. With this threshold imposed, $\gamma = 0.513 \pm 0.001$ and $\delta = 0.255 \pm 0.044$ (compared to NT predictions of $\gamma = 0.50$ and $\delta = 0.25$). The critical stress scaling remains essentially unchanged, with $\gamma' = 0.608 \pm 0.029$.

stress, and thus saturated stress, depends only on the bendability of the ribbon. We anticipate that these facts uncovered by our simulations, and the introduction of bendability parameter in the context of twisted sheets, will prove useful in further theoretical development of scaling laws.

ML was supported by the Ford Foundation Predoctoral Fellowship and the National Science Foundation Graduate Research Fellowship Program under grant no. DGE-1745303. AK was supported by National Science Foundation grant DMR-2005090. CHR was partially supported by the Applied Mathematics Program of the U.S. DOE Office of Science Advanced Scientific Computing Research under contract number DE-AC02-05CH11231.

* (she/her) mleembruggen@g.harvard.edu

† jovana@sas.upenn.edu

‡ akudrolli@clarku.edu

§ chr@math.wisc.edu

- [1] E. Cerda and L. Mahadevan. Geometry and Physics of Wrinkling. *Physical Review Letters*, 90(7):074302, February 2003.
- [2] Dayong Chen, Shengqiang Cai, Zhigang Suo, and Ryan C. Hayward. Surface Energy as a Barrier to Creasing of Elastomer Films: An Elastic Analogy to Classical Nucleation. *Physical Review Letters*, 109(3):038001, July 2012. Publisher: American Physical Society.
- [3] Jean-Christophe G  minard, Roberto Bernal, and Francisco Melo. Wrinkle formations in axi-symmetrically stretched membranes. *European Physical Journal E: Soft matter and biological physics*, 15(2):117, 2004.
- [4] Benny Davidovitch, Robert D. Schroll, Dominic Vella, Mokhtar Adda-Bedia, and Enrique A. Cerda. Prototypical model for tensional wrinkling in thin sheets. *Proceedings of the National Academy of Sciences*, 108(45):18227–18232, November 2011. Publisher: Proceedings of the National Academy of Sciences.
- [5] B. Davidovitch, R. D. Schroll, and E. Cerda. Nonperturbative model for wrinkling in highly bendable sheets. *Physical Review E*, 85(6):066115, June 2012.
- [6] Peter Bella and Robert V. Kohn. Wrinkles as the Result of Compressive Stresses in an Annular Thin Film. *Communications on Pure and Applied Mathematics*, 67(5):693–747, May 2014.
- [7] Jiangshui Huang, Megan Juszkievicz, Wim H. de Jeu, Enrique Cerda, Todd Emrick, Narayanan Menon, and Thomas P. Russell. Capillary Wrinkling of Floating Thin Polymer Films. *Science*, 317(5838):650–653, August 2007. Publisher: American Association for the Advancement of Science.
- [8] D. Vella, M. Adda-Bedia, and E. Cerda. Capillary wrinkling of elastic membranes. *Soft Matter*, 6(22):5778–5782, November 2010. Publisher: The Royal Society of Chemistry.
- [9] Douglas P. Holmes and Alfred J. Crosby. Draping Films: A Wrinkle to Fold Transition. *Physical Review Letters*, 105(3):038303, July 2010.
- [10] Miguel Pi  neirua, Nana Tanaka, Beno  t Roman, and Jos  

- Bico. Capillary buckling of a floating annulus. *Soft Matter*, 9(46):10985–10992, November 2013. Publisher: The Royal Society of Chemistry.
- [11] K. Bugra Toga, Jiangshui Huang, Kevin Cunningham, Thomas P. Russell, and Narayanan Menon. A drop on a floating sheet: boundary conditions, topography and formation of wrinkles. *Soft Matter*, 9(34):8289–8296, August 2013. Publisher: The Royal Society of Chemistry.
- [12] Dominic Vella, Jiangshui Huang, Narayanan Menon, Thomas P. Russell, and Benny Davidovitch. Indentation of Ultrathin Elastic Films and the Emergence of Asymptotic Isometry. *Physical Review Letters*, 114(1):014301, January 2015. Publisher: American Physical Society.
- [13] Finn Box, Dominic Vella, Robert W. Style, and Jerome A. Neufeld. Indentation of a floating elastic sheet: geometry versus applied tension. *Proceedings of the Royal Society A: Mathematical, Physical and Engineering Sciences*, 473(2206):20170335, October 2017. Publisher: Royal Society.
- [14] Gregory M. Grason and Benny Davidovitch. Universal collapse of stress and wrinkle-to-scar transition in spherically confined crystalline sheets. *Proceedings of the National Academy of Sciences*, 110(32):12893–12898, August 2013. Publisher: Proceedings of the National Academy of Sciences.
- [15] Evan Hohlfeld and Benny Davidovitch. Sheet on a deformable sphere: Wrinkle patterns suppress curvature-induced delamination. *Physical Review E*, 91(1):012407, January 2015.
- [16] Benny Davidovitch, Yiwei Sun, and Gregory M. Grason. Geometrically incompatible confinement of solids. *Proceedings of the National Academy of Sciences*, 116(5):1483–1488, January 2019. Publisher: Proceedings of the National Academy of Sciences.
- [17] Elodie Aumaitre, Sebastian Knoche, Pietro Cicuta, and Dominic Vella. Wrinkling in the deflation of elastic bubbles. *The European Physical Journal E*, 36(3):22, March 2013.
- [18] Albert Edward Green. The elastic stability of a thin twisted strip—II. *Proceedings of the Royal Society of London. Series A - Mathematical and Physical Sciences*, 161(905):197–220, July 1937. Publisher: Royal Society.
- [19] David J. Crispino and Richard C. Benson. Stability of twisted orthotropic plates. *International Journal of Mechanical Sciences*, 28(6):371–379, January 1986.
- [20] C. D. Coman and A. P. Bassom. An asymptotic description of the elastic instability of twisted thin elastic plates. *Acta Mechanica*, 200(1-2):59–68, September 2008.
- [21] Julien Chopin, Vincent Démery, and Benny Davidovitch. *Roadmap to the Morphological Instabilities of a Stretched Twisted Ribbon*, pages 137–189. Springer Netherlands, Dordrecht, 2016.
- [22] Huy Pham Dinh, Vincent Démery, Benny Davidovitch, Fabian Brau, and Pascal Damman. From Cylindrical to Stretching Ridges and Wrinkles in Twisted Ribbons. *Physical Review Letters*, 117(10):104301, September 2016. Publisher: American Physical Society.
- [23] Julien Chopin and Arshad Kudrolli. Helicoids, Wrinkles, and Loops in Twisted Ribbons. *Physical Review Letters*, 111(17):174302, October 2013.
- [24] Madelyn Leembruggen, Jovana Andrejevic, Arshad Kudrolli, and Chris H. Rycroft. Computational model of twisted elastic ribbons. *Physical Review E*, 108:015003, 2023.
- [25] Julien Chopin and Romildo T. D. Filho. Extreme contractility and torsional compliance of soft ribbons under high twist. *Phys. Rev. E*, 99:043002, Apr 2019.
- [26] Joseph D. Paulsen, Evan Hohlfeld, Hunter King, Jiangshui Huang, Zhanlong Qiu, Thomas P. Russell, Narayanan Menon, Dominic Vella, and Benny Davidovitch. Curvature-induced stiffness and the spatial variation of wavelength in wrinkled sheets. *Proceedings of the National Academy of Sciences*, 113(5):1144–1149, February 2016. Publisher: Proceedings of the National Academy of Sciences.
- [27] H. S. Seung and David R. Nelson. Defects in flexible membranes with crystalline order. *Physical Review A*, 38(2):1005–1018, July 1988.
- [28] Allen Van Gelder. Approximate simulation of elastic membranes by triangulated spring meshes. *Journal of Graphics Tools*, 3(2):21–41, 1998.
- [29] Bryn Lloyd, Gabor Székely, and Matthias Harders. Identification of Spring Parameters for Deformable Object Simulation. *IEEE Transactions on Visualization and Computer Graphics*, 13(5):1081–1094, September 2007.
- [30] Eitan Grinspun, Anil N. Hirani, Mathieu Desbrun, and Peter Schröder. Discrete shells. In *Proceedings of the 2003 ACM SIGGRAPH/Eurographics symposium on Computer animation*, SCA '03, pages 62–67, Goslar, DEU, July 2003. Eurographics Association.
- [31] Rasmus Tamstorf and Eitan Grinspun. Discrete bending forces and their Jacobians. *Graphical Models*, 75(6):362–370, November 2013.
- [32] Jovana Andrejevic and Chris H. Rycroft. Simulation of crumpled sheets via alternating quasistatic and dynamic representations. *Journal of Computational Physics*, 471:111607, 2022.
- [33] Zhanlong Qiu. *Morphology of Thin Sheets in the Lame Setup and Beyond*. PhD thesis, University of Massachusetts Amherst, March 2017.